Free surface flow driven by a rotating end wall in a stationary cylinder : Structure of the axisymmetric baseflow

W. YANG[a, b, c, 1], J. CHERGUI[a], Y. FRAIGNEAU[a]
I. DELBENDE[a, b, 2], L. MARTIN WITKOWSKI[a, b, 3]

a. LIMSI-CNRS, Bât 508 Rue John von Neumann 91405 Orsay cedex, France
b. UPMC-Paris VI, 4 place Jussieu 75005 Paris, France
c. FAST UMR 7608, 23-25 rue Jean Rostand Parc-Club Orsay Université 91405 Orsay cedex, France

Résumé :

L'écoulement en rotation engendré par le fond tournant d'une cuve cylindrique fixe partiellement remplie d'un liquide est étudié numériquement. Pour des vitesses de rotation élevées, la surface du liquide se déforme fortement et des instabilités brisant la symétrie de révolution peuvent apparaître. L'étude axisymétrique de l'écoulement, nous a permis de révéler sa structure qui est composée d'une colonne centrale de fluide tournant à la même vitesse que le fond de la cuve et d'une zone périphérique qui s'articule en quatre couches limites. Ces fines couches entourent un coeur où la vitesse de rotation est quasi constante. Cela nous encourage à discuter la pertinence des modèles existants qui ont été utilisés jusqu'à présent pour analyser les instabilités de cet écoulement.

Abstract :

We study the steady free-surface flow of a viscous liquid layer contained in a cylinder with a rotating bottom and a fixed lateral wall. When the disk rotates at large speed, the free surface deforms strongly and three-dimensional instability patterns (rotating polygons) or sloshing motions can arise. In order to get some insight on their formation mechanisms, a study of the axisymmetric base flow is carried out numerically. The flow structure consists of a well-known central fluid column entrained in a motion of solid-body rotation at the disk angular velocity. The fluid region situated at the periphery reveals a complex structure as it is found to be surrounded by four boundary layers. This leads us to discuss the relevance of existing base-flow models used for instability studies of this flow configuration.

Mots clefs : rotating flow, free surface, axisymmetric

1. yang@fast.u-psud.fr
2. ivan.delbende@upmc.fr
3. laurent.martin_witkowski@upmc.fr

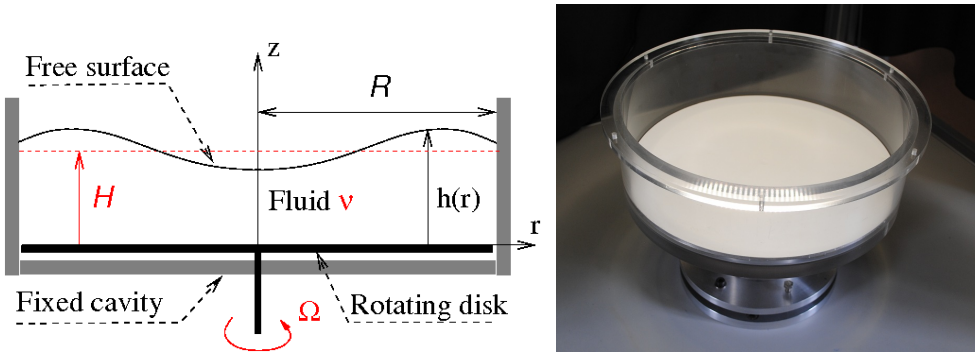

FIGURE 1 – System and experimental setup.

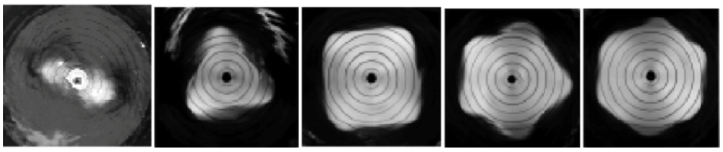

FIGURE 2 – Polygonal instability patterns (first seen in [8], but illustrations come from [9]).

1 Introduction

Communities of geophysical and industrial flows have always found common interests in studying the stability of rotating flows in academic configurations. A rotating disk at the bottom of a fixed cavity partially filled with a fluid is a good example of such configurations. A typical setup is shown in figure 1. In this context, numerous experimental studies have emerged since the early 1990s.

In an early work, Vatistas [8] found that polygons changing from ellipse to hexagon (see Figure 2) appeared at the free surface depending on the angular velocity Ω of the disk and the initial liquid height H. These patterns rotate in the same direction as the disk but with a smaller angular velocity. Since then, other experiments confirmed those results. For instance, the same phenomena were also observed by another group of researchers in Danemark [4] as well as a group from Japan [6].

Several theories have been proposed to explain the azimuthal symmetry breaking. The formation of the polygons was related to point vorticies by Vatistas *et al.* in [9]. However, Bergmann *et al.* [1], measured the rotation velocities of each vortices and revealed that the power of point vortices is too weak to acquire the observed rotating speed of the entire pattern. Tophøj *et al.* [7] explained the rotating polygonal instability as a result of gravity waves and centrifugal waves's interaction (thanks to a linear stability analysis on a potential vortex flow). Fabre and Mougel [2] extended this work to a more general case with a Rankine vortex model as a baseflow.

The aim of the present work is to get a better understanding of the structure of the baseflow with the help of numerical axisymmetric simulations. This may serve in the future as a basis for linear stability analysis.

2 Flow parameters and numerical method

The system is presented in figure 1. It consists of a layer of liquid of density ρ_l and kinematic viscosity ν, placed in a cylindrical container of radius R, over a disk of the same radius rotating at angular velocity Ω.

The surface tension at the interface of air-liquid is denoted as σ and the gravity acceleration as g. All length, velocity, density and pressure variables are respectively non-dimensionalized by R, $R\Omega$, ρ_l and $\rho_\mathrm{l} R^2\Omega^2$.

Relative to the liquids considered here (water), the dynamic viscosity of air is such that $\mu_\mathrm{air}/\mu_\mathrm{l} \sim 2.10^{-2}$ and its density such that $\rho_\mathrm{air}/\rho_\mathrm{l} \sim 10^{-3}$. This allows us to neglect the tangential stress exerted by the air on liquid surface and the pressure variations in the air. As a consequence, the dynamics of the air phase is not taken into account in this study. Following non-dimensional parameters can be constructed :

$$Re = \frac{R^2\Omega}{\nu}\,, \quad Fr = \frac{R\Omega^2}{g}\,, \quad We = \frac{\rho_\mathrm{l}\Omega^2 R^3}{\sigma}\,, \quad a = \frac{H}{R}\,. \tag{1}$$

The shape of the interface can be substantially modified by the surface tension, but this is true only at low Weber number values (lower than several hundreds). In most experiments, the Weber number is always larger than 1000 and is no longer a relevant parameter of the problem. In what follows, the Weber number is thus kept constant at $We = 1236.6$ as in the experiment of Bergmann (as explained below) and we focus on the influence of the Reynolds number and the Froude number on the flow.

The computations are carried out by a code named *ROSE* which is developed in our group to compute steady axisymmetric flows efficiently using a Newton-Raphson procedure. The stationary Navier–Stokes equations are written in streamfunction-vorticity formulation. The code uses curvilinear grid to adapt to the deformed interface and second-order spatial discretization. Only the liquid phase is computed. The method is described in [5] and we found that taking into account the surface tension was very helpful in stabilizing the iterative process.

3 Results

3.1 Flow structure

We present the typical flow structure on a reference case (figure 12 of Ref. [1]). To our knowledge, it is the only experiment with quantitative measurement of flow velocity. It is unfortunately restricted to measures obtained on the free surface. The experimental parameters are $H/R = 0.1856$, $Fr = 0.2464$, $We = 1236.6$ and Reynolds number $Re = 132\ 860$. The computations are carried out at much lower values of Reynolds number (up to $Re = 20000$) but we claimed that most of the structure for high Reynolds number values is revealed. Isocontours of the streamfunction and azimuthal velocity component are shown in figure 3 left. The central part of the liquid is in solid-body rotation at the disk angular velocity, while at the periphery the angular velocity decreases and a recirculating region occurs, best seen in a meridional plane.

We characterize the length L of the peripheral region as the radial distance between the point of maximum azimuthal velocity along the free surface at $r = r_\mathrm{max}$ and the side wall : $L = R - r_\mathrm{max}$ (see figure 3 right). For this large Reynolds number values, this region is seen to be delineated by four boundary layers : one at the disk, one along the end wall, one at the free surface, and one along the central part in body rotation.

The flow structure at steady state is schematically represented in figure 4. The free surface height at steady state is denoted by $h(r)$. Quantities $h_0 = h(0)$ and $h_1 = h(1)$ are introduced. The characterization of the four boundary layers will be addressed further.

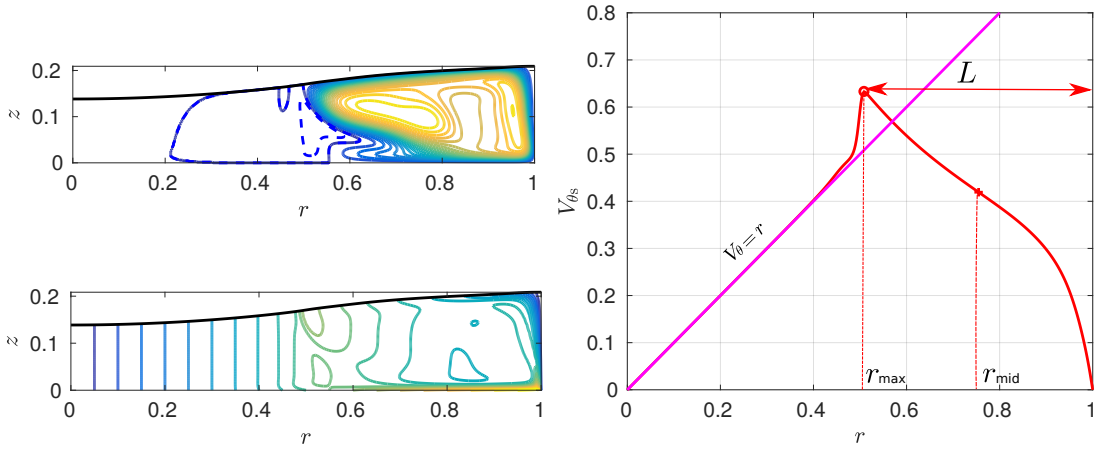

FIGURE 3 – Left : Contours of the streamfunction ψ (top left) and azimuthal velocity component V_θ (bottom left) for $H/R = 0.1856$, $Fr = 0.2464$ and $Re = 20\,000$. For ψ, 20 equally spaced contours between 0 and $\psi_{\max} = 0.0024$ as well as 2 equally spaced dashed contours between $\psi_{\min} = -1.485 \times 10^{-4}$ and 0 are used. For V_θ, 20 contours are equally spaced between 0 and 1. Right : azimuthal velocity component at the free surface $V_{\theta s}$ as a function of r and definition of several positions.

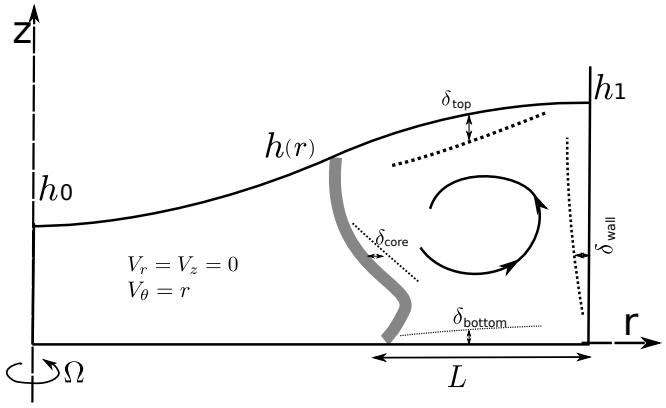

FIGURE 4 – Sketch of the flow in a meridional plane. The fluid follows the disk at the same rotation rate (solid body rotation) in the central part (left of the gray band). A meridional recirculation with four boundary layers is present at the periphery.

3.2 Effects of Reynolds number

First, we investigate the effects of the Reynolds number on the flow structure. Here, a small constant Froude number $Fr = 0.01$ is taken. We show in the following section that, apart from deforming the free surface, increasing the Froude number does not change significantly the flow structure. To clarify the relation between the length L and the Reynolds number, steady simulations for a series of Reynolds numbers from 10 and 20 000 was conducted. It is seen in figure 5 that $L(Re)$ has a three stage evolution. L increases abruptly almost linearly for $100 \leq Re \leq 700$ (regime 1), is then roughly constant on a short range up to $Re \approx 1600$ (regime 2). It then smoothly increases and saturates at a slightly higher level (regime 3).

We chose three Reynolds numbers, $Re = 300, 1200, 10\,000$, located respectively in each of the above regimes. Figure 6 gives the corresponding profiles of the azimuthal velocity component V_θ as a function

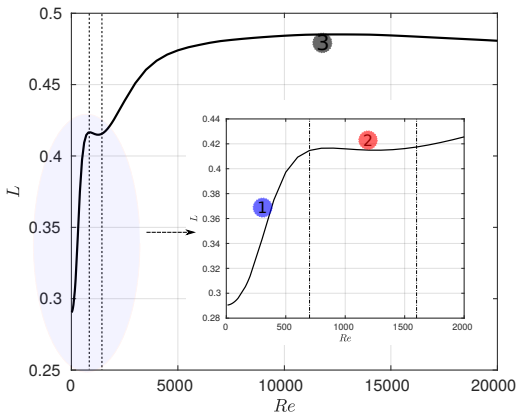

FIGURE 5 – Evolution of the size L of the peripheral region as a function of Re. $Fr = 0.01$, $H/R = 0.1856$

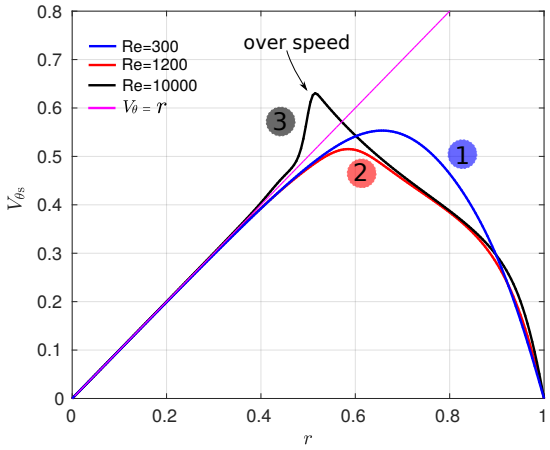

FIGURE 6 – Typical profiles of $V_{\theta s}$ as a function of r for each regime.

of r along the free surface. The three velocity profiles are virtually indistinguishable for a radius smaller than 0.4. They are superimposed with the curve $V_\theta = r$ so that all the regimes behave identically in the inner part : a solid-body rotating at the angular speed of the disk. The main differences between the regimes are in the peripheral region. If L is considered to start from one point in the region of solid-body rotation, its value would likely be almost constant in figure 5. The definition based on the maximum azimuthal velocity, always underestimates the length of the outer region but it makes the different regimes more obvious in figure 5. The blue curve 1 corresponding to $Re = 300$ illustrates a regime with a moderate convective flow. The red curve 2, at $Re = 1200$, is in the regime of appearance of boundary layers. The gray curve 3, for $Re = 10\,000$, is characteristic of the observed overshoot in the azimuthal velocity for large Reynolds values. A more complete understanding of the regimes is also provided by taking a close examination of the isocontours of streamfunction and azimuthal velocity component in figure 7. The density of the contours which are linearly spaced gives insight on the boundary layers' formation. Finally, the radial profile of V_z at $z = h_0/2$ and the axial profile of rV_r at $r = r_{\text{mid}}$ which are plotted in figure 8 are also helpful in the analysis. The radius r_{mid} at which the profiles are plotted is $r_{\text{mid}} = r_{\text{max}} + L/2$.

The transition between these different regimes can be explained as follow. For very low values of Reynolds number, the flow is entirely dominated by viscous effects. The equation for the azimuthal component of velocity reduces to a purely diffusive equation without source term and with a non homogeneous boundary condition on the disk. The azimuthal velocity is of the order of magnitude the velocity of the disk. The meridional velocities (radial and axial components) are also purely diffusive having only homogeneous boundary condition. They are driven by the only source term which is the axial variation of the azimuthal velocity. Meridional components are weak compared to the azimuthal one. Indeed, the maximum value of the streamfunction scales as $\alpha \cdot Re$ with $\alpha \approx 10^{-5}$

This viscous regime is barely visible in figure 5. One can only observe at the beginning of regime 1 a very small plateau as Re tends to zero. Removing all convective terms in our solver leads to find $L = 0.29$ which is the starting point of regime 1. As the value of the Reynolds number increases, the meridional flow strengthens but continues to scale linearly with Re up to $Re \approx 300$. Along the free surface, the negative radial velocity convects low azimuthal velocity from the periphery toward the axis. It has the effect of weakening the azimuthal velocity and thus L increases. Progressively, the meridional

flow interacts with the azimuthal velocity and modifies its own source term.

As the Reynolds number increases, one could expect that the meridional flow expands and eventually reaches the axis. However, the convection is damped by forces that prevent motion perpendicular to the rotation axis (this is related to Taylor-Proudman theorem). Along the free surface, as r decreases, the radial velocity is forced to decrease to zero as it reaches the central region. The flow by continuity turns to be mainly axial. Thus L results from an equilibrium between these two phenomena and reaches again a plateau.

L increases again at the beginning of the third regime. This is due to the effect of conservation of angular momentum that is responsible for the overshoot observed in figure 6. In this higher Reynolds regime, dissipation is quite weak especially far from any walls so that one can consider to some extent that $rV_{\theta \mathrm{s}} = \text{cte}$ which is true in the inviscid limit. The maximum is again shifted toward the axis by this effect, which causes L to increase.

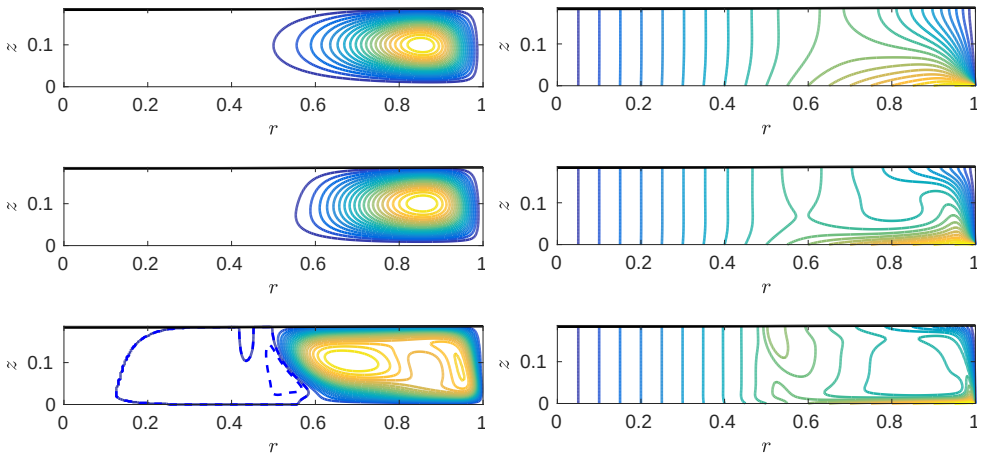

FIGURE 7 – Contours of the streamfunction (left) and azimuthal velocity component (right) for $Fr = 0.01$, $Re = 300, 1200, 10000$ from top to bottom. 20 equally spaced solid contours between 0 and $\psi_{\max} = (0.00355, 0.0074, 0.00345)$ and 2 equally spaced dashed contours between $\psi_{\min} = (0, 0, -1.996 \times 10^{-4})$ and 0 ; V_θ is positive, with 20 equally spaced contours between 0 and 1.

To quantify the boundary layers, we have defined the following length scales :

- δ_{bottom}, the distance between the maximal rV_r position (circle symbols in Fig 8 right) and the disk at $r = r_{\mathrm{mid}}$;
- δ_{wall}, the distance between the maximal V_z position (square symbols in the Fig 8 left) and the side wall at $z = h_0/2$;
- δ_{top}, the distance between the interface and the inflexion point of the rV_r profile ('+' symbols in Fig 8 right) at $r = r_{\mathrm{mid}}$.
- δ_{core}, the distance between $r_{\max}$ and the minimal V_z position ('*' symbol in Fig 8 left) at $z = h_0/2$.

The influence of Reynolds number on the thickness of the boundary layers is shown in figure 9. The thickness of the boundary layers, except that of the core, undergo similar tendency : a plateau before $Re = 300$ and a decrease afterwards. If the scaling of each boundary layer thickness is far from being clear and understood, it is quite satisfactory that the beginning of regime 2 is corroborated by these plots. It must be noted that the definitions of δ are questionable, especially for δ_{core} as it is a layer not directly

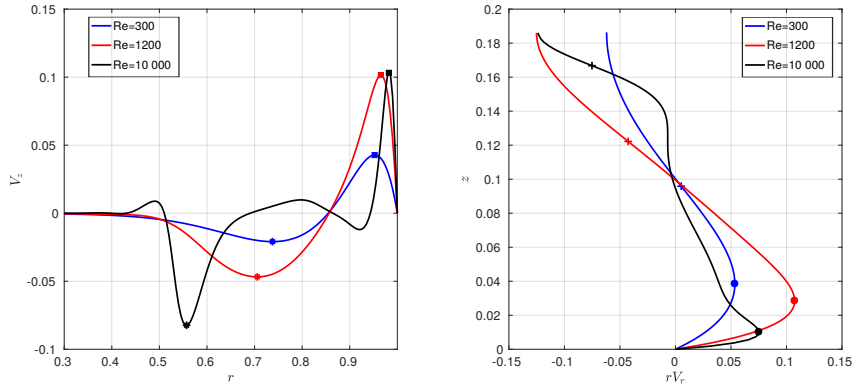

FIGURE 8 – $Fr = 0.01$. Left : axial velocity component V_z as a function of r at $z = h_0/2$; Right : rV_r as a function of z at $r = r_{\text{mid}}$.

related to a frontier of the fluid. Its behaviour is presented for the sake of completeness but it is likely that a different criterium has to be found.

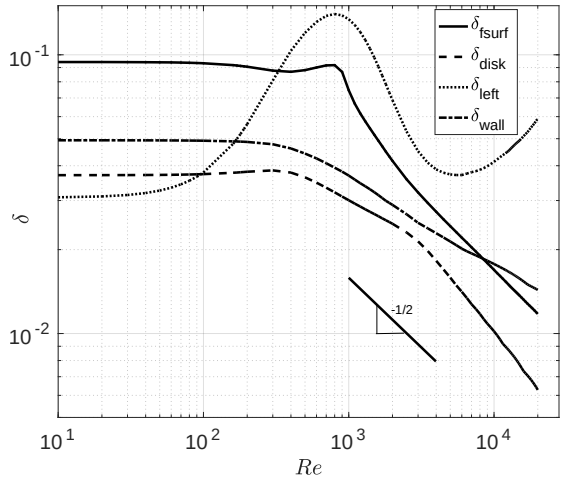

FIGURE 9 – Dependency of boundary layers thickness on the Reynolds number for $H/R = 0.1856$, $Fr = 0.01$.

3.3 Effects of Froude number at large Reynolds number

In order to study the effects of Froude number, we compare three different Froude number values : $Fr = 0.01, 0.2464, 1.0$ while keeping other parameters constant : $Re = 10000$, $We = 1236.6$, $H/R = 0.1856$. According to figure 10 (left) and without surprise, the first effect of increasing the value of Froude number is to strongly modify the shape of the free surface. For $Fr = 1$, h_0 is yet close to 0. This effect is expected as the Froude number measures the competition between centrifugal and gravity acceleration. Less obvious is the fact that the flow structure is almost the same for all Froude numbers even though the free surface shape was strongly modified. The central region with solid body rotation extend over the same radius. The vortex breakdown [3] attached to the interface are weakened but their location is barely changed.

This similarity in the flow structure becomes even more evident when the velocity profiles are superim-

posed. In figure 10 (right), the axial coordinate is normalized. The profile for the velocity component V_θ and rV_r are plotted as a function of $z/h_{0.8}$ at $r = 0.8$ where $h_{0.8} = h(r = 0.8)$ is the interface height at $r = 0.8$. These profiles also illustrate the effect of Taylor-Proudman theorem. An almost z-independent region where the meridional flow is extremely weak and V_θ reaches a constant value. This region is surrounded by two boundary layers, one above the disk and the other under the free surface.

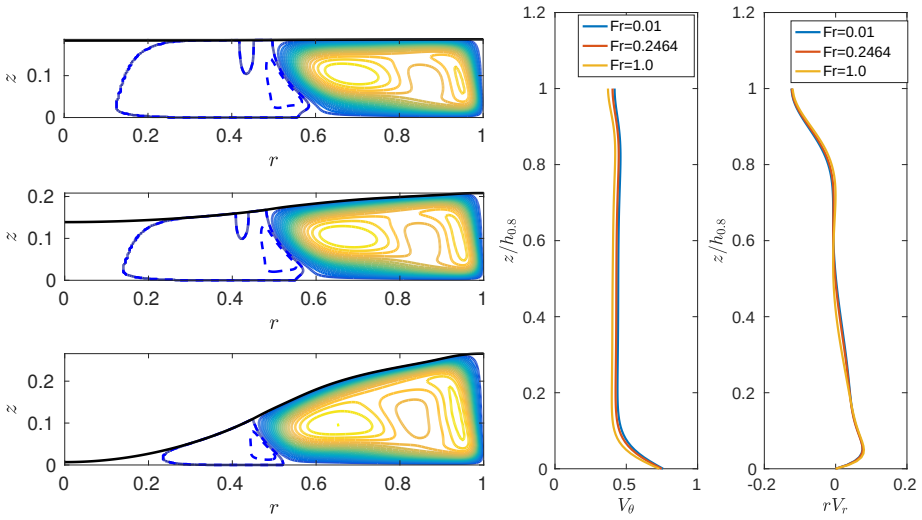

FIGURE 10 – $Re = 10000, H/R = 0.1856, We = 1263.6$, $Fr = 0.01, 0.2464, 1.0$ from top to bottom. Left : 20 equally spaced solid contours of stream function between 0 and $\psi_{\max} = (0.0035, 0.0035, 0.0035)$ and 2 equally spaced dashed contours between $\psi_{\min} = (-1.996 \times 10^{-4}, -1.979 \times 10^{-4}, -1.836 \times 10^{-4})$ and 0 ; Right : V_θ and rV_r profiles as functions of $z/h_{0.8}$ at $r = 0.8$.

4 Conclusion

This study is a first step toward a better understanding of the complex flow generated by a rotating disk at the bottom of fixed cavity partially filled with liquid. For moderate Reynolds number, many of the features of the flow is explained and are almost straightforward to understand. For high Reynolds number, we have shown the structure of the flow with a central region in solid body rotation and a peripheral region holding a z-independent core surrounded by four boundary layers. This structure is independent of the Froude number or in other words independent of the shape of the free surface. However, the scaling of the boundary layers remains unclear. A good comprehension of this regime is a necessary step as it will allow us to improve the baseflow model that have been proposed up to now and give more insight to the instability mechanisms of the azimuthal symmetry breaking observed in experiments.

Our computations can be compared to the experiment of Bergmann *et al.* (fig. 12 in [1]) in the following way. The shape of the free surface, even if there is no real quantitative values besides a picture, is in fair agreement. There is also a good agreement on the radius of the central region and as corollary a perfect agreement on the azimuthal velocity (solid body rotation). However, the overshoot of V_{θ_s} due to the conservation of angular momentum is not observed experimentally and V_{θ_s} close to the wall also differs. We believe that the region close to the wall is likely to be difficult to be measured precisely in the experiment but the overshoot should be captured easily. A possible explanation is that a flow instability (not necessarily strong enough to modify the free surface shape) redistribute the angular momentum

through a three dimensional mechanism. Our present computation is not able to capture this mechanism. This point is under investigation.

Références

[1] R. Bergmann, L. Tophøj, T. A. M. Homan, P. Hersen, A. Andersen, and T. Bohr. Polygon formation and surface flow on a rotating fluid surface. *J. Fluid Mech.*, 679 :415–431, 7 2011.

[2] D Fabre and J Mougel. Generation of three-dimensional patterns through wave interaction in a model of free surface swirling flow. *Fluid Dyn. Res.*, 46(6) :061415, 2014.

[3] M.A. Herrada, V.N. Shtern, and J.M. Lopez-Herrera. Off-axis vortex breakdown in a shallow whirlpool. *Phys. Rev. E*, 87 :063016(8), 2013.

[4] T. R. N. Jansson, M. P. Haspang, K. H. Jensen, P. Hersen, and T. Bohr. Polygons on a rotating fluid surface. *Phys. Rev. Lett.*, 96 :174502, 2006.

[5] L. Kahouadji and L. Martin Witkowski. Free surface due to a flow driven by a rotating disk inside a vertical cylindrical tank : Axisymmetric configuration. *Phys. Fluids*, 26 :072105(17), 2014.

[6] T. Suzuki, M. Iima, and Y. Hayase. Surface switching of rotating fluid in a cylinder. *Phys. Fluids*, 18 :101701(4), 2006.

[7] L. Tophøj, J. Mougel, T. Bohr, and D. Fabre. Rotating polygon instability of a swirling free surface flow. *Phys. Rev. Lett.*, 110 :194502, May 2013.

[8] G. H. Vatistas. A note on liquid vortex sloshing and Kelvin's equilibria. *J. Fluid Mech.*, 217 :241–248, 1990.

[9] Georgios H. Vatistas, Hamid A. Abderrahmane, and M. H. Kamran Siddiqui. Experimental confirmation of Kelvin's equilibria. *Phys. Rev. Lett.*, 100 :174503, Apr 2008.